Magnetic Resonance in Medicine 62:1574–1584 (2009)

Accelerating SENSE Using Compressed Sensing

Dong Liang,[1] Bo Liu,[1,2] JiunJie Wang,[3] and Leslie Ying[1*]

Both parallel MRI and compressed sensing (CS) are emerging techniques to accelerate conventional MRI by reducing the number of acquired data. The combination of parallel MRI and CS for further acceleration is of great interest. In this paper, we propose a novel method to combine sensitivity encoding (SENSE), one of the standard methods for parallel MRI, and compressed sensing for rapid MR imaging (SparseMRI), a recently proposed method for applying CS in MR imaging with Cartesian trajectories. The proposed method, named CS-SENSE, sequentially reconstructs a set of aliased reduced-field-of-view images in each channel using SparseMRI and then reconstructs the final image from the aliased images using Cartesian SENSE. The results from simulations and phantom and in vivo experiments demonstrate that CS-SENSE can achieve a reduction factor higher than those achieved by SparseMRI and SENSE individually and outperform the existing method that combines parallel MRI and CS. Magn Reson Med 62:1574–1584, 2009. © 2009 Wiley-Liss, Inc.

Key words: SENSE; compressed sensing; SparseMRI; Sparse-SENSE; CS-SENSE

MRI speed is usually limited by the large number of samples needed along the phase-encoding direction. In conventional MRI using Fourier encoding, the required number of samples is determined by the field of view (FOV) and the resolution of the image based on the Shannon sampling theory. To accelerate conventional MRI, both parallel MRI (pMRI) and compressed sensing MRI (CS-MRI) are advanced techniques to reduce the number of acquired data. In pMRI, due to the availability of multichannel coils, the MR images can be reconstructed from multichannel *k*-space data sampled below the Nyquist sampling rate. Standard reconstruction methods include SENSE (1), simultaneous acquisition of spatial harmonics (SMASH) (2), generalized autocalibrating partially parallel acquisitions (GRAPPA) (3), etc. Theoretically, the maximum reduction factor can be up to the number of channels under ideal conditions. However, this maximum usually cannot be achieved due to practical limitations such as noise and imperfect coil geometry. CS-MRI is based on CS theory (4-9), a new framework for data sampling and signal recovery. CS-MRI takes advantage of the fact that MRI meets two conditions of CS. One is the MR images are sparse or compressible after certain transformations. The other is the Fourier encoding is incoherent with these sparse transformations. Therefore, the MR images can be reconstructed using a nonlinear convex program from data sampled at a rate close to their intrinsic information rate, which is well below the Nyquist rate. CS-MRI methods include SparseMRI for Cartesian trajectories (10) and methods for other trajectories (11,12).

Because pMRI and CS-MRI reduce sampling based on different ancillary information (channel sensitivities for pMRI and image sparseness for CS), it is desirable to combine pMRI and CS for further reduction. SparseSENSE and its equivalence (13-16) have been proposed as a straightforward combination method. This method reconstructs images from the multichannel data, using the same nonlinear convex program as that employed in SparseMRI, except that the Fourier encoding is replaced by the sensitivity encoding (comprising Fourier encoding and sensitivity weighting). However, the incoherence between the sensitivity encoding matrix and any sparsifying transform, which is one of prerequisites of CS, has not been explored theoretically in SparseSENSE. It has been stated (15), but without mathematical proof, that the sensitivity encoding matrix is not as incoherent with the standard sparsifying transform (e.g., wavelet) as the Fourier matrix. This is partially because the sensitivity encoding matrix is not an orthonormal basis primarily considered in the CS theory and can vary from scan to scan due to its dependence on channel sensitivities. In this paper, we propose a novel method named CS-SENSE, which has been partially presented (17), to combine CS-MRI and pMRI for the Cartesian case with guaranteed incoherence. CS-SENSE sequentially carries out CS reconstruction (using SparseMRI) for the aliased image of each channel and Cartesian SENSE for the final unfolded image. Because the encoding matrix in the first CS reconstruction is the Fourier matrix, as in conventional MR imaging, incoherence with identity matrix or the fine scales of a wavelet transform has been proven (6). Our simulation and experimental results show that CS-SENSE can achieve a reduction factor higher than those achieved by SparseMRI and SENSE individually and can outperform SparseSENSE in terms of resolution.

THEORY

Summary of SENSE

SENSE is one of the standard reconstruction methods for parallel imaging. For arbitrary trajectories, the general SENSE equation is (18)

$$\mathbf{Ef} = \mathbf{d} \qquad [1]$$

where $\mathbf{d}$ is the vector formed from the *k*-space data acquired in all channels, $\mathbf{f}$ is the unknown vector defining the desired full FOV image to be computed, both with a lexicographical row ordering of the two-dimensional array

[1]Department of Electrical Engineering and Computer Science, University of Wisconsin–Milwaukee, Milwaukee, Wisconsin, USA

[2]MR Engineering, GE Healthcare, Waukesha, Wisconsin, USA

[3]Department of Medical Imaging and Radiological Sciences, ChangGung University, Tao-Yuan, Taiwan

*Correspondence to: L. Ying, Department of Electrical Engineering and Computer Science, University of Wisconsin–Milwaukee, 3200 N. Cramer Street, Milwaukee, WI 53211. E-mail: leiying@uwm.edu

Received 28 August 2008; revised 23 June 2009; accepted 6 July 2009.

DOI 10.1002/mrm.22161

Published online 25 September 2009 in Wiley InterScience (www.interscience.wiley.com).

© 2009 Wiley-Liss, Inc.

components, and **E** is the sensitivity encoding matrix whose entries are

$$\mathbf{E}_{\{l,m\},n} = e^{-i2\pi(k_x x + k_y y)} S_l(x,y) \quad [2]$$

where k_x and k_y denote the k-space sampling position for the m^{th} element in **d**, (x, y) denotes the pixel position for the n^{th} element in **f**, and s_l is the sensitivity profile of the l^{th} receiver channel.

Summary of CS

CS (4-9) is a new mathematical framework for signal sampling and recovery. It allows faithful recovery of a transform-sparse signal **x** of size n from its linear measurements $\mathbf{y} = \mathbf{\Phi x}$ whose size m is much less than n, by solving a convex program

$$\min_{\mathbf{x}} \|\mathbf{\Psi x}\|_1 \text{ s.t. } \quad \mathbf{\Phi x} = \mathbf{y} \quad [3]$$

where Φ is the CS encoding matrix, Ψ a sparsifying transform, and $\|\mathbf{x}\|_1$ the ℓ_1 norm, defined as the sum of the complex modulus $\|\mathbf{x}\|_1 = \Sigma_i|_i|$. To achieve faithful recovery from very few measurements, some sufficient conditions need to be satisfied (6,7): (a) the signal is sparse after a known sparsifying transform Ψ, (b) the encoding matrix Φ is incoherent with the sparsifying transform Ψ, and (c) the measurements exceed the minimum requirement, which is usually two to five times the sparsity of $\mathbf{\Psi x}$.

Although these conditions are not exactly satisfied in practical sampling and reconstruction problems, the signal can still be recovered with good fidelity under relaxed conditions when sufficient incoherent measurements are acquired. For example, the signals may not be strictly sparse but only compressible instead (i.e., sparse after thresholding the transform coefficients), and the measurements **y** may contain some noise **e** whose ℓ_2 norm is bounded by a constant ϵ, i.e.,

$$\mathbf{y} = \mathbf{\Phi x} + \mathbf{e} \quad \|\mathbf{e}\|_2 \le \varepsilon \quad [4]$$

Under this circumstance, the signal can be recovered by

$$\mathbf{x}^* = \arg\min_{\mathbf{x}} \|\mathbf{\Psi x}\|_1 \text{ s.t.} \|\mathbf{\Phi}_{\mathbf{x}-\mathbf{y}}\|_2 \le \varepsilon \quad [5]$$

and the reconstruction error is proved to be bounded by (8)

$$\|\mathbf{x}^* - \mathbf{x}\|_2 \le c_1 \frac{\|\mathbf{x} - \mathbf{x}^S\|_1}{\sqrt{S}} + c_2\varepsilon \quad [6]$$

which is proportional to the noise level ε and the approximation error between the signal **x** and its closest S-sparse signal $\mathbf{x}^S$. The c_1 and c_2 are the constants whose values are smaller with a higher level of incoherence and a larger number of measurements (8). In summary, under practical conditions, the CS reconstruction quality depends on the incoherence, the number of measurements, measurement noise, and compressibility of the image.

Summary of SparseMRI and SparseSENSE

SparseMRI (10) is a practical technique to apply CS to conventional Cartesian MRI. Conventional Fourier imaging meets the relaxed CS conditions: most MR images are compressible with identity transform or wavelet transform and the Fourier encoding is sufficiently incoherent with these sparsifying transforms (19). The SparseMRI method fully samples the k-space along the readout direction and randomly undersamples the k-space along the phase-encoding direction, using a variable-density sampling scheme with denser sampling near the center of the k-space. The randomly generated sampling pattern with the lowest peak transform point spread function (10) is chosen for data acquisition. The final image is reconstructed from the undersampled k-space data by solving a constrained convex optimization problem (10):

$$\min_{\mathbf{f}}(\|\mathbf{\Psi f}\|_1 + \alpha\|\mathbf{f}\|_{\text{TV}}) \text{ s.t.} \|\mathbf{F}_u\mathbf{f} - \mathbf{d}_u\|_2 \le \varepsilon \quad [7]$$

where **F** and **d** are the Fourier encoding matrix and the corresponding vector formed from the fully sampled k-space data, respectively, the subscript u denotes a random subset of the rows, and $\|\mathbf{f}\|$ is the total variation, defined as $\|\mathbf{f}\|_{\text{TV}} = \Sigma\sqrt{|\nabla_x f|^2 + |\nabla_y f|^2}$ with ∇_x and ∇_y being the finite difference along x and y respectively, and $|\cdot|$ being the complex modulus (20). This formulation requires the image to be sparse in both the transform domain defined by Ψ and the finite difference domain, whose tradeoff is controlled by the constant α. The constrained minimization in Eq. 7 is usually achieved by solving an equivalent unconstrained regularization problem:

$$\arg\min_{\mathbf{f}}\{\|\mathbf{F}_u\mathbf{f} - \mathbf{d}_u\|_2^2 + \lambda(\|\mathbf{\Psi f}\|_1 + \alpha\|\mathbf{f}\|_{\text{TV}})\} \quad [8]$$

where λ is the regularization parameter to be selected to make the solution of Eq. 8 the same as that of Eq. 7 (10).

SparseSENSE or its equivalence (13-16) are a direct extension of SparseMRI to apply CS to SENSE. It employs the same random sampling scheme as that of SparseMRI and solves a similar constrained convex optimization problem:

$$\min_{\mathbf{f}}(\|\mathbf{\Psi f}\|_1 + \alpha\|\mathbf{f}\|_{\text{TV}}) \text{ s.t.} \|\mathbf{Ef} - \mathbf{d}\|_2 \le \varepsilon \quad [9]$$

The difference lies in that the Fourier encoding matrix in SparseMRI is replaced by the sensitivity encoding matrix **E** which consists of both Fourier encoding and sensitivity weighting. The major issue with this method is that the incoherence between the encoding matrix **E** and the sparsifying basis Ψ such as the identity or wavelet has not yet been explored. It is still well accepted that **E** will be less incoherent with the sparsifying basis than the Fourier encoding matrix (15).

Proposed CS-SENSE

When the sampling is on a uniform Cartesian grid, the sensitivity encoding in Eq. 1 can be decomposed into two sequential linear operations (21). The first one is the sensitivity modulation $\tilde{\mathbf{C}}$, where the original full FOV image **f**,

weighted by different sensitivities from all channels, is folded to generate a set of aliased images with reduced FOV $\mathbf{f}^A$, i.e.,

$$\tilde{\mathbf{C}}\mathbf{f} = \mathbf{f}^A \quad [10]$$

The second one is Fourier transform of each aliased image

$$\mathbf{F}\mathbf{f}_l^A = \mathbf{d}_l \quad [11]$$

where $\mathbf{f}_l^A$ is the aliased image of the l^{th} channel with reduced FOV, $\mathbf{d}_l$ the reduced k-space data from the l^{th} channel. The image vector $\mathbf{f}^A$ is a stack of vectors $\mathbf{f}_l^A$ from all channels. The basic Cartesian SENSE reconstruction (1) takes advantage of the above two-step formulation. It initially Fourier transforms the acquired data to obtain a set of aliased images and then unfolds these images by solving the linear equation of Eq. 10.

The proposed CS-SENSE method also takes advantage of the decoupled formulation and uses a similar framework, except that SparseMRI replaces the Fourier transform procedure. This replacement is based on the fact that the aliased reduced FOV images $\mathbf{f}_l^A$ are still sparse under the same transform, if the original full FOV image is sparse under a certain transform. In data acquisition, the same random sampling scheme as that for SparseMRI is employed to further undersample the data along the phase-encoding direction that is already undersampled for the reduced FOV. One out of 20 randomly generated sampling patterns with the lowest peak transform point spread function is chosen to acquire the data and can be reused for other image acquisitions when the sparsifying transform and the image size stay the same. With this random undersampling, Eq. 11 becomes underdetermined and is represented as

$$\mathbf{F}_u\mathbf{f}_l^A = \mathbf{d}_{u,l} \quad [12]$$

where $\mathbf{d}_{u,l}$ is the undersampled k-space data from the l^{th} channel and is a subset of $\mathbf{d}_l$. In reconstruction, the aliased image $\mathbf{f}_l^A$ of each channel can be solved by

$$\min_{\mathbf{f}_l^A} (\|\mathbf{\Psi}\mathbf{f}_l^A\|_1 + \alpha\|\mathbf{f}_l^A\|_{\text{TV}}) \text{ s.t.} \|\mathbf{F}_u\mathbf{f}_l^A - \mathbf{d}_{u,l}\|_2 \le \varepsilon \quad [13]$$

Similar to Lustig et al. (10), due to its computational complexity, the above constrained minimization is solved by its equivalence instead

$$\arg\min_{\mathbf{f}_l^A} \{\|\mathbf{F}_u\mathbf{f}_l^A - \mathbf{d}_{u,l}\|_2^2 + \lambda(\|\mathbf{\Psi}\mathbf{f}_l^A\|_1 + \alpha\|\mathbf{f}_l^A\|_{\text{TV}})\} \quad [14]$$

where the parameter λ is determined by solving Eq. 14 with different values of λ and choosing one so that $\|\mathbf{F}_u\mathbf{f}_l^A - \mathbf{d}_{u,l}\|_2 \approx \varepsilon$. With the aliased images from all channels, the desired full FOV image $\mathbf{f}$ can be reconstructed pixel by pixel using the image domain Cartesian SENSE method. No regularization is used here in the SENSE step, though it can be easily incorporated later. It is easy to see that the net reduction factor R of CS-SENSE is equal to the product of the reduction factor R_1 in SparseMRI and the reduction factor R_2 in Cartesian SENSE, i.e., $R = R_1 \times R_2$.

The proposed CS-SENSE method is different from SparseSENSE in several aspects. First, CS-SENSE randomly undersamples the k-space which is already reduced for the aliased images, while SparseSENSE randomly undersamples the full k-space. Second, CS-SENSE sequentially applies CS and SENSE, where the nonlinear CS step solves a set of underdetermined equations. In contrast, SparseSENSE directly solves an overdetermined equation using the nonlinear CS algorithm when the reduction factor is less than the number of channels. Since the CS theory primarily considers underdetermined equations, SparseSENSE is better regarded as a regularized SENSE with random trajectories. Unlike the CS theory where the sparse constraint helps to pick the best one among an infinite number of solutions to an underdetermined equation, the ℓ_1 regularization in SparseSENSE never gives a solution satisfying the overdetermined data consistency exactly; there always exists a tradeoff between the data consistency and the sparsity. Finally, and most important, the incoherence condition required in CS is guaranteed in CS-SENSE when the image is sparse or compressible in image domain or in wavelet domain, but is not necessarily satisfied in SparseSENSE. CS-SENSE uses the same Fourier encoding matrix as SparseMRI does, whose incoherence with the identity and wavelet transforms has been proven (4-6). In contrast, the encoding matrix in SparseSENSE depends on the coil sensitivities and is not an orthonormal basis primarily considered in the CS theory. It is very difficult to verify the incoherence between the sensitivity encoding and the sparse transformation basis such as wavelet since it can vary from scan to scan.

MATERIALS AND METHODS

The proposed CS-SENSE method was evaluated on four datasets: simulated data (with different level of noise), scanned phantom data, and T_1-weighted human brain data (on axial and sagittal planes). All reconstruction methods were implemented in MATLAB (MathWorks, Natick, MA) on a workstation (Hewlett-Packard, Palo Alto, CA) with a 2.33-GHz central processing unit and 2-GB random-access memory. Nonlinear conjugate gradient (10) was used to solve Eq. 14. The sum-of-square (SoS) reconstruction from the fully sampled data was used as the reference image for comparison. To quantitatively evaluate the performance of the proposed method, the normalized mean square error (NMSE) (22) between the reconstructed and the reference images was calculated. It provides a combined metric for image noise, artifacts, and loss of resolution. All reconstructed images for the same dataset are shown individually on the same scale for visual evaluations of image noise, artifacts, and resolution.

Simulation

A 256×256 numerical phantom was constructed and used as the original image. The phantom is piecewise smooth and is thus strictly sparse (i.e., most coefficients are exactly zero) in finite difference. The objective of this

simulation is to demonstrate that exact reconstruction of a strictly sparse image is possible using CS-SENSE when there are sufficient noise-free measurements. In addition, the simulation is to show how the reconstruction quality is affected with increasing undersampling and noise. The simulated *k*-space data were generated by Fourier transforming the sensitivity-weighted images and undersampling according to the random sampling pattern. The sensitivities of an eight-channel coil were simulated using the Biot-Savart law (23). Different levels of Gaussian noise were added to the simulated *k*-space data to investigate the effect of noise. The average signal-to-noise ratios (SNR) were infinity (no noise), 30, 15, and 7.5. The reduction factors take $R = 2 \times 2$, 3×2, and 4×2, where the first factor R_1 is the reduction factor of SparseMRI and R_2 is the reduction factor of SENSE. The combination of R_1 and R_2 used here is chosen to give the best reconstruction among several possible combinations for the same reduction factor. In reconstruction, only the total variation penalty was used to enforce the sparsity in finite difference. All results include reconstructions from SparseSENSE for comparison. The normalized NMSEs were calculated as a function of the reduction factor and SNR.

Phantom Experiment

The objective of the phantom experiment is to demonstrate that CS-SENSE can generate high-quality reconstructions from highly reduced, actually scanned data when the image well satisfies the sparsity requirement. A phantom that consists of well-defined, piecewise-smooth structures was used. A T_1-weighted scan was performed on the phantom using a two-dimensional spin echo sequence on a 3T commercial scanner (GE Healthcare, Waukesha, WI) with an eight-channel torso coil (echo time/pulse repetition time = 11/300 ms, 18-cm FOV, eight slices, 256×256 matrix). The full *k*-space data were acquired and the central 32 fully sampled phase encodings were used to estimate the channel sensitivity profiles. Specifically, a set of low-resolution images was generated from the central *k*-space data weighted by a cosine taper window (24). These images were then normalized by their SoS reconstruction and weighted by a mask that set to zeros the regions with low image intensity. The masking step is to reduce the sensitivity estimation error caused by the low-intensity region, as pointed out by Pruessmann et al. (1). The reduced data were generated by manually removing some data to simulate reduction factors of 2×2, 3×2, and 4×2. Only these reduced data were used for final reconstruction, excluding the fully sampled data for sensitivity estimation. Since the phantom is sparse by itself, the identity matrix was used as the sparse transformation Ψ in the CS-SENSE reconstruction. For comparison, SparseSENSE and two other competing methods were also used for reconstruction. One approach was VD-SENSE (25) with ℓ_2 regularization, whose regularization function is defined as $\|\Delta \mathbf{f}\|_2 = \Sigma|\Delta_x f|^2 + |\Delta_y f|^2$ as in Block et al. (11) and Ying et al. (26), and the other used SparseMRI for a full FOV image in each channel and a SoS combination. The latter approach is similar to Marinelli et al. (27), except that the joint sparsity was not employed here due to its inhibitive computational requirement.

In Vivo Human Brain Imaging Experiment

This experiment is to examine the performance of CS-SENSE when applied to in vivo images that are usually not as sparse as phantoms but compressible with wavelet and finite-difference transforms. Two sets of in vivo human brain data (axial and sagittal) were acquired. The axial data set was from a 3T commercial scanner (GE Healthcare, Waukesha, WI) with an eight-channel head coil (In Vivo, Gainesville, FL) using a two-dimensional T_1-weighted spin echo protocol (TE/TR = 11/700 ms, 22-cm FOV, 10 slices, 256×256 matrix). The sagittal data set was on a 1.5 T Siemens Avanto system with a four-channel head coil using a two-dimensional T_1-weighted spin echo protocol (TE/TR = min full/500 ms, 24-cm FOV, 256×256 matrix). Informed consent was obtained from the volunteer in accordance with the institutional review board policy. The sagittal image is less compressible (i.e., larger compression error with the same compression ratio) than the axial image due to numerous fine details, making it a more challenging CS-SENSE reconstruction. The Daubechies-4 wavelet (28) was used as the sparse transformation Ψ in Eq. 14. Similar to the phantom experiment, the SoS reconstruction was used as the reference for comparison, and the central 32 fully sampled phase encodings were used to estimate the channel-sensitivity profiles. Different reduction factors were used for each reconstruction. The reconstructed images and their corresponding error images were shown for comparison.

RESULTS

All images are labeled by the method used on the top left corner and the reduction factor on the top right corner. "Ref" denotes the reference image, "A" the CS-SENSE, "B" the SparseSENSE, "C" the SparseMRI followed by SoS, and "D" the VD-SENSE with ℓ_2 regularization.

Simulation

Figure 1 shows the reconstructed image of the numerical phantom by CS-SENSE and SparseSENSE in the ideal noise-free case. At a reduction factor of 4, both methods are able to reconstruct the original image exactly. No difference can be identified visually. As the net reduction factor increases, the reconstruction qualities of both CS-SENSE and SparseSENSE deteriorate gracefully and the artifacts gradually show up. At a high reduction factor of 8, both reconstructions have visible undersampling artifacts. The CS-SENSE reconstruction is seen to be smoother. Since the exact sensitivity profiles are used in simulation, the SENSE step of CS-SENSE only amplifies the artifacts from the previous step without introducing additional artifacts.

Figure 2 shows the reconstructed images for $R = 4$ when different levels of noise are added to the measurements. It is seen that at all noise levels, CS-SENSE well preserves the image structures, with only random noise added on the structures. The larger the measurement noise is, the larger the reconstruction noise is. This observation agrees with the CS reconstruction error bound in Eq. 6, which increases with the measurement noise level when other con-

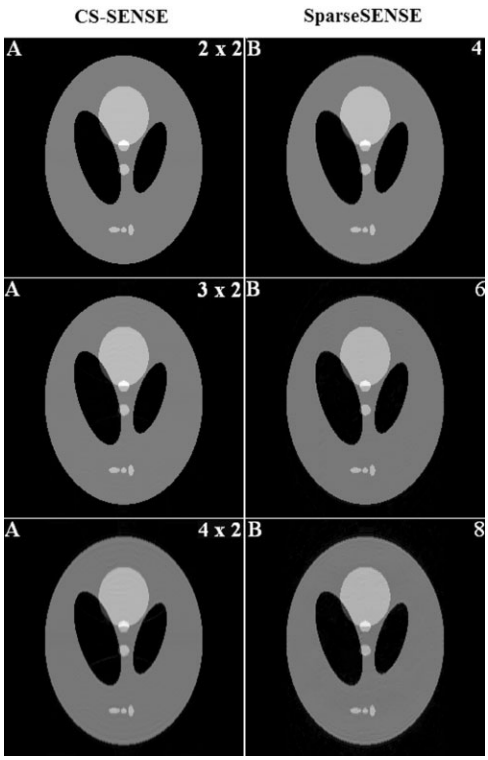

FIG. 1. Images reconstructed from a set of simulated, eight-channel, noise-free data with different net reduction factors. The left column is for CS-SENSE (denoted as **A**) and the right column is for SparseSENSE (denoted as **B**), with the reduction factors shown on the top right corner of each image.

ditions are kept the same. In contrast, the measurement noise not only causes reconstruction noise but also introduces blocky artifacts in SparseSENSE reconstructions, which is obvious at low SNRs. This is better explained in the context of regularization. At low SNRs, it is known that regularization has to suppress large noise at the cost of increased artifacts and blurriness.

Table 1 shows the NMSEs of both methods, with different reduction factors ($R = 4, 6, 8$) and SNRs (7.5, 15, and 30). The unit of 10^{-002} was used. Although NMSE is too general to provide a precise metric for the image quality, the table provides a quantitative measure for the overall errors. As expected, both methods perform better as the SNR increases and/or the reduction factor decreases. CS-SENSE is superior to SparseSENSE in terms of NMSE with the same reduction factor and SNR.

Phantom Experiment

Figure 3 shows the reconstructions from the scanned phantom data, with the zoomed "comb" region on the bottom left corner of each image to reveal more details. At a reduction factor of $R = 4$, both CS-SENSE and SparseSENSE are able to reconstruct an image visually the same as the reference image. In contrast, SparseMRI followed by SoS has visible undersampling artifacts. This is because the method does not utilize the sensitivity information and it is difficult to achieve a high reduction factor of 4 using SparseMRI alone. VD-SENSE with ℓ_2 regularization has more noise. As the reduction factor becomes larger ($R = 6$), the superior performance of CS-SENSE becomes more visible. The CS-SENSE reconstruction is able to preserve the image resolution, while other reconstructions become blurry, which is clearly shown in the zoomed "comb" region. Even at a reduction factor as high as 8 (equal to the number of channels), the CS-SENSE reconstruction only slightly loses resolution, while more details are lost in all other reconstructions. In both the CS-SENSE and SparseSENSE reconstructions, artifacts becomes more visible as the reduction factor increases from 4 to 8, but noise still keeps low even at $R = 8$. In contrast, the noise in VD-SENSE with ℓ_2 regularization and the artifacts in SparseMRI followed by SoS increase more with the reduction factor. The phantom results suggest that the SNR in a real experiment is usually good enough for CS-SENSE to achieve a high reduction factor in reconstructing a highly sparse image.

In Vivo Human Brain Imaging Experiment

Figure 4 shows the axial reconstructions with a zoomed region of interest on the bottom right corner of each image.

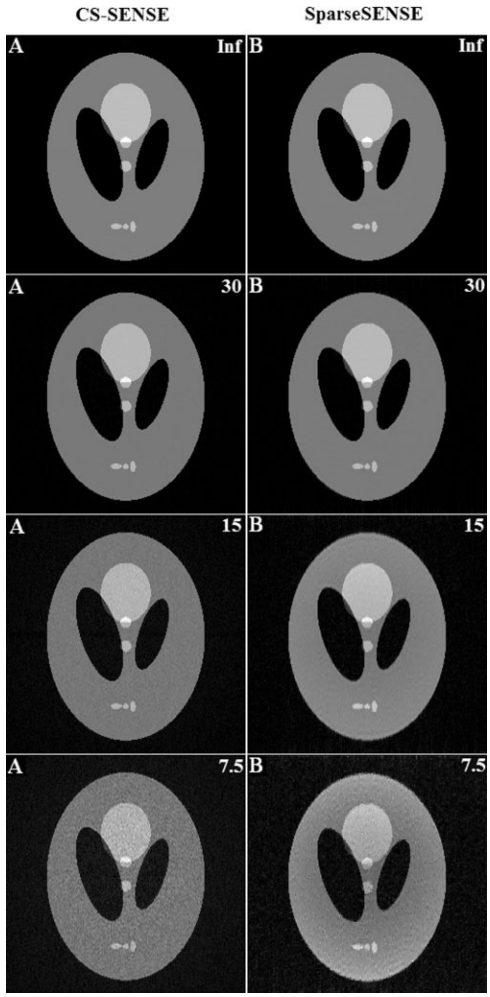

FIG. 2. Images reconstructed from a set of simulated eight-channel data with different levels of noise for $R = 4$. The left column is for CS-SENSE (denoted as **A**) and the right column is for SparseSENSE (denoted as **B**), with the SNRs shown on the top right corner of each image.

Table 1
NMSEs ($\times 10^{-002}$) of Reconstructions Using Simulation Data

R Factor	4 (2 × 2)			6 (3 × 2)			8 (4 × 2)		
SNR (dB)	7.5	15	30	7.5	15	30	7.5	15	30
CS-SENSE	2.22	0.77	0.05	2.34	0.75	0.19	2.63	0.79	0.34
SparseSENSE	3.09	0.90	0.12	3.74	1.34	0.35	3.91	1.75	0.56

For better visualization, all the corresponding error images are also shown in Fig. 5 on the same scale. At a reduction factor of $R = 4$, both CS-SENSE and SparseMRI reconstructions are very similar to the reference image visually. However, unlike the phantom results, both begin to lose resolution, with the SparseSENSE image being slightly more blurry than the CS-SENSE one (shown in the zoomed region of interest). SparseMRI followed by SoS has visible undersampling artifacts. VD-SENSE with ℓ_2 regularization is the noisiest among all the methods shown. As the reduction factor becomes larger ($R = 6$), all images become more blurry and show undersampling artifacts, which is clear in the error images shown in Fig. 5. The large values at object edges shown in the error images indicate a serious loss of resolution. The structured ripples within the objects in the error images indicate undersampling artifacts. In comparison, CS-SENSE preserves more details with fewer undersampling artifacts than the other methods do. For an even higher reduction factor, all methods fail to reconstruct an acceptable image.

Figures 6 and 7 show the sagittal reconstructions with the zoomed cerebellum on the bottom right corner of each image and the corresponding error images, respectively. Due to the large number of details in the image, none of the methods are able to preserve the resolution with $R = 3$ or 4. All reconstructions show undersampling artifacts. In comparison, CS-SENSE preserves much more detail than the other methods, as shown in the zoomed region of interest. From the error images, it is seen that the errors of CS-SENSE primarily come from the spatial varying noise due to the noise amplification by the large *g*-factor (1). This is because the *g*-factor for the four-channel data is larger than that for the eight-channel data, although the reduction factor R_2 for the SENSE step is kept the same. The images of the other methods show a significant amount of artifacts and serious loss of resolution.

The in vivo experiment demonstrates that CS-SENSE requires more measurements to be successful as the image has more details (i.e., is less compressible). This observation agrees with the CS reconstruction error bound in Eq.

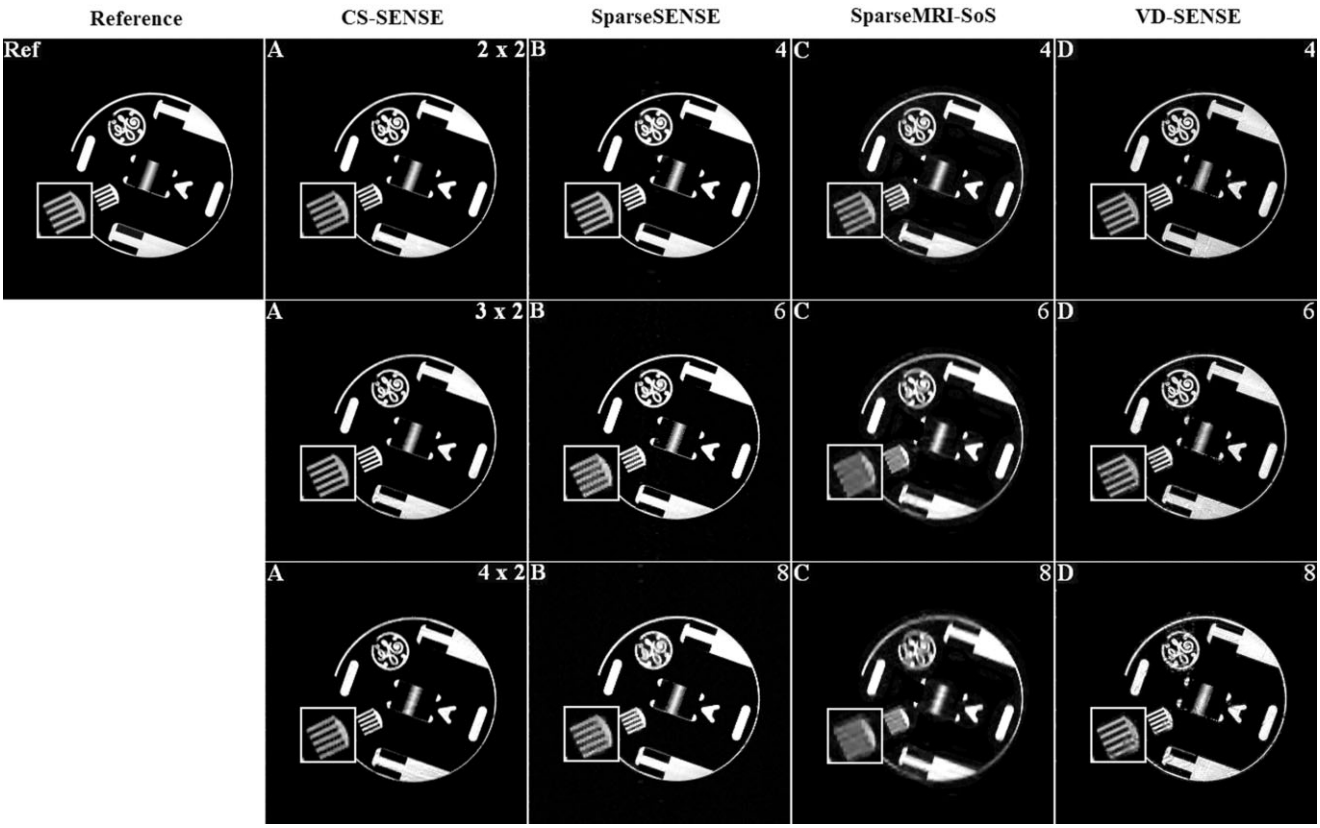

FIG. 3. Phantom images reconstructed using CS-SENSE **(A)**, SparseSENSE **(B)**, SparseMRI followed by SoS **(C)**, and VD-SENSE with ℓ_2 regularization **(D)** from a set of eight-channel scanned data with different net reduction factors shown on the top right corners. The corresponding "comb" region was zoomed to reveal details.

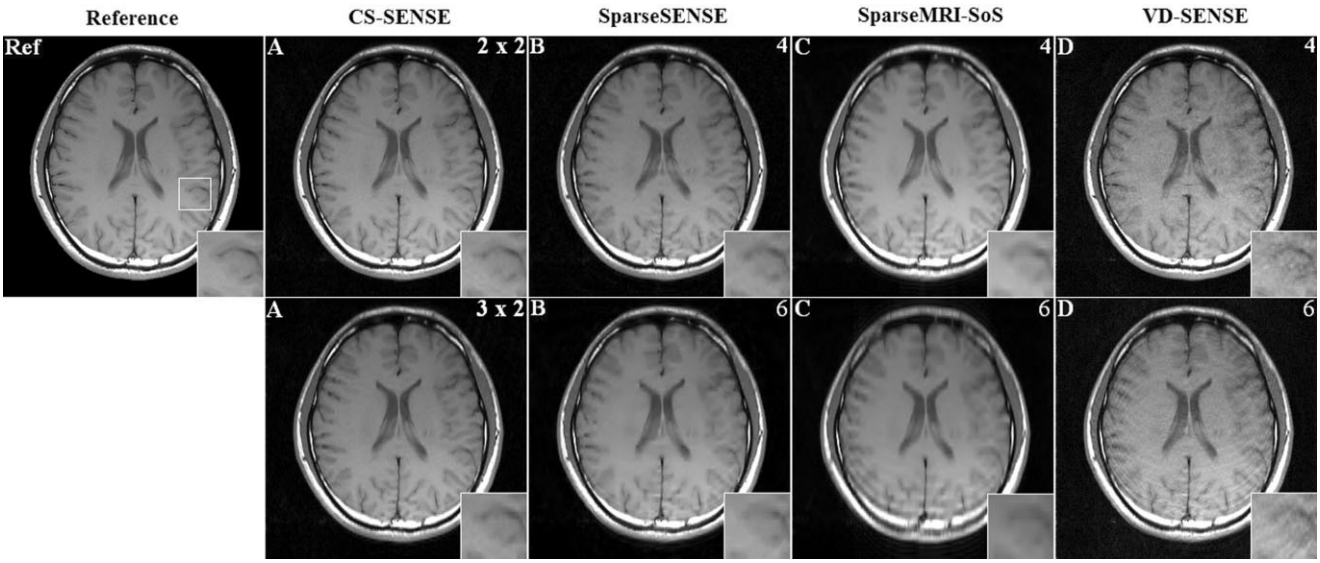

FIG. 4. Axial brain images reconstructed using CS-SENSE **(A)**, SparseSENSE **(B)**, SparseMRI followed by SoS **(C)**, and VD-SENSE with ℓ_2 regularization **(D)** from a set of eight-channel scanned data with different reduction factors shown on the top right corners. A region of interest (enclosed by a rectangle in the reference image denoted as "Ref") was zoomed and shown at the bottom right corner of each image.

6, which increases with the compression error. Compared to the competing methods, CS-SENSE is able to preserve many more details without a significant compromise in SNR and artifacts.

Table 2 shows the NMSEs of both the axial and sagittal reconstructions as a function of reduction factors. CS-SENSE has the lowest NMSEs among the competing methods with the same reduction factor, which agrees with the observations in Figs. 4-7.

DISCUSSION

In this paper, a novel method, CS-SENSE, is proposed to further accelerate parallel imaging. This method is compared with SparseSENSE and other existing imaging methods using computer simulation, scanned phantom, and in vivo brain data. The experimental results demonstrate that the proposed CS-SENSE method is superior to the existing competing methods, especially in preserving resolution. The superior resolution is primarily due to the decoupling of CS and SENSE in the proposed method. Although all methods used for comparison in Results section have "regularization" capability, the regularization of CS-SENSE occurs only in the CS step, which shares a fraction of the total reduction factor. As known in regularization, the lower the reduction factor is, the less the resolution has to be traded to suppress the undersampling artifacts and noise. Since the CS-SENSE only regularizes at a low reduction factor, the resolution does not have to be compromised as much as in other methods where the total reduction factor is considered in regularization. On the other hand, since regularization is not used in the SENSE step of CS-SENSE, the resolution is not reduced, but the noise can be amplified in this step. This may result in slightly larger

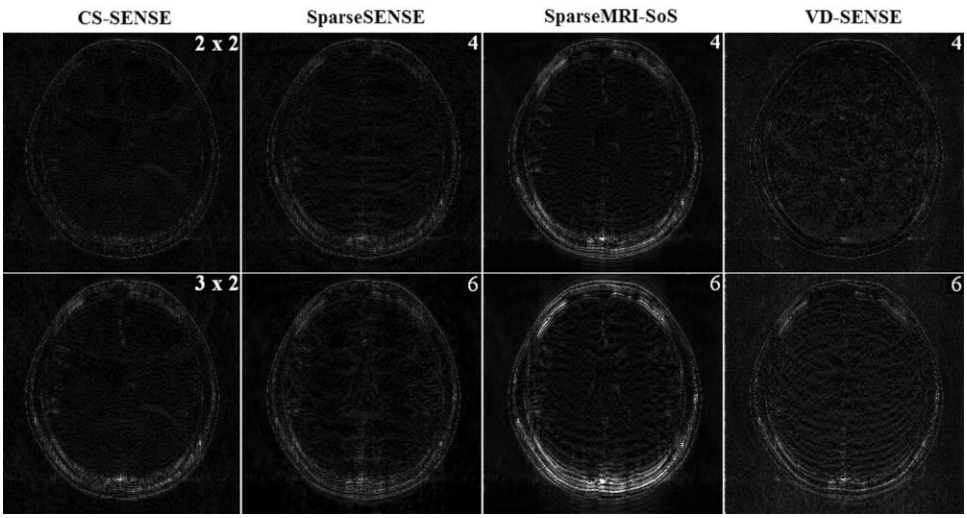

FIG. 5. Error images corresponding to the axial reconstructions in Fig. 4.

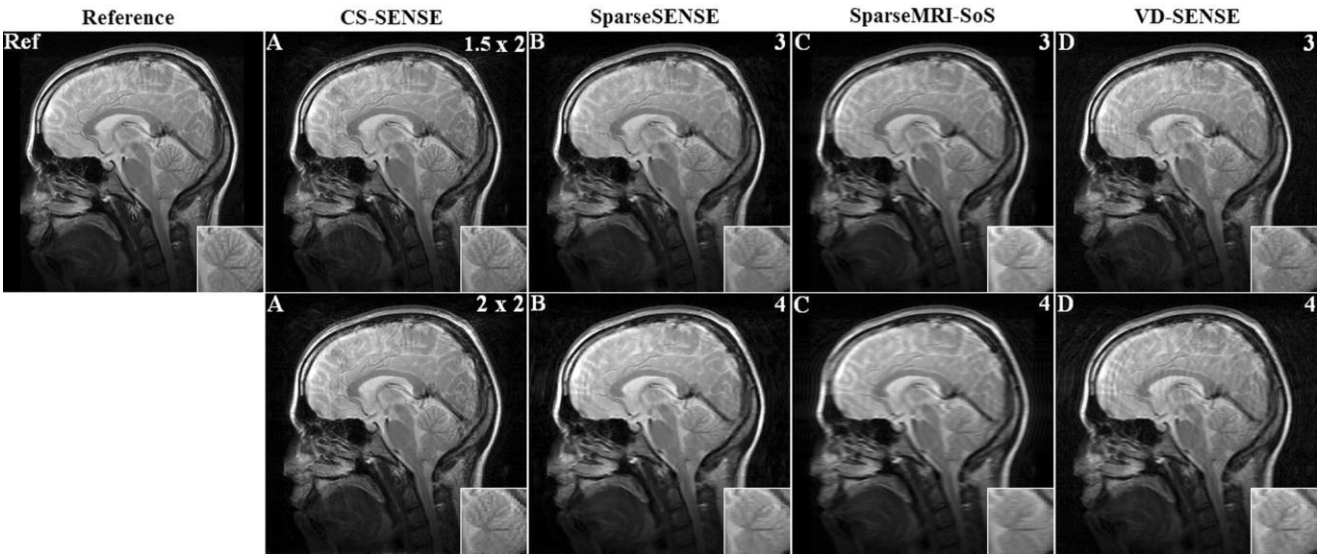

FIG. 6. Sagittal brain images reconstructed using CS-SENSE **(A)**, SparseSENSE **(B)**, SparseMRI followed by SoS **(C)**, and VD-SENSE with ℓ_2 regularization **(D)** from a set of four-channel scanned data with different reduction factors shown on the top right corners. The zoomed cerebellum was shown on the bottom right corner of each image to show CS-SENSE is able to preserve much more detail than the other methods.

noise in CS-SENSE than the competing methods when the *g*-factor is large.

Reconstruction Errors

The CS-SENSE method consists of two steps, generating the intermediate aliased images using SparseMRI and reconstructing the desired image from these aliased images using SENSE. As a result, the reconstruction error of CS-SENSE comes from both steps.

In the first step of SparseMRI, three major factors affect the reconstruction quality with the same reduction factor: the incoherence level, measurement noise, and the sparsity of the image after transformation. The effect of different noise levels is demonstrated in the computer simulation. The reconstruction only becomes noisier with increased measurement noise. Noise does not introduce artifacts. The effect of image sparsity is demonstrated in the phantom and in vivo experiments. For example, for high-quality reconstruction, the reduction factor can be as high as 6 for the very sparse phantom, about 4 for the moderately sparse axial brain image with wavelet transform, and barely 3 for the sagittal brain image with many details. It suggests that in vivo images, which usually have larger approximation error than the phantoms when made to be sparse, will lead to reconstructions of lower quality. In other words, to achieve the same image quality, in vivo images need more measurements than the phantoms do.

The sparsity of the image depends on the sparsifying transforms, as demonstrated in Lustig et al. (10). For example, both brain images in the experiments are not sparse by themselves but can be sparse with a wavelet transform. In other words, to achieve the same sparsity, the identity

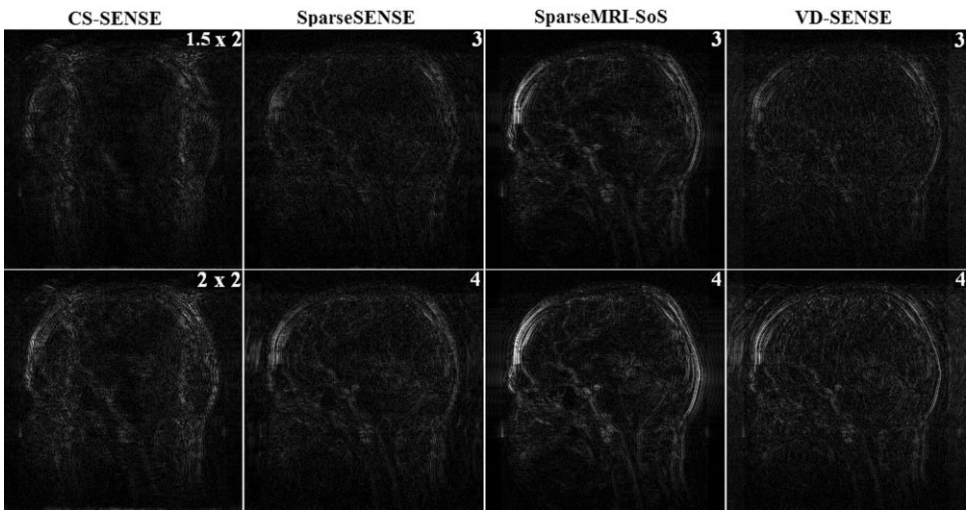

FIG. 7. Error images corresponding to the sagittal reconstructions in Fig. 6.

Table 2
NMSEs ($\times 10^{-002}$) of Reconstructions Using In Vivo Data

R Factor, data set sagittal	1.5 × 2, Sagittal	2 × 2		3 × 2, Axial
		Sagittal	Axial	
CS-SENSE 0.62	0.62	0.91	0.25	0.83
SparseSENSE0.65	0.65	1.13	0.59	1.06
SparseMRI-SoS	1.22	1.89	1.81	2.91
VD-SENSE+l_2	0.82	1.41	0.69	1.51

transform results in much larger approximation error than the wavelet transform. Therefore, according to the error bound in Eq. 6, the use of wavelet transform in CS reconstruction from brain data leads to much less reconstruction error. The CS reconstruction is expected to benefit from the future development of sophisticated transforms that give even sparser representations than the currently used wavelet and identity transforms.

In the second step of SENSE, two factors affect the reconstruction quality: the accuracy of sensitivity profiles and the *g*-factor. It is known that inaccurate sensitivity profiles directly cause aliasing artifacts in basic SENSE (22). As a result, CS-SENSE also suffers from the sensitivity error. All error images of CS-SENSE show some fold-over aliasing artifacts. As with SENSE, the artifacts can be reduced by improving the sensitivity accuracy. Figure 8 shows that the CS-SENSE reconstruction improves when the sensitivity profiles are estimated from 128 encodings instead of 32.

Both noise and artifacts in the first step will propagate to the second step of SENSE. In SENSE, the *g*-factor map has been used to characterize the spatial dependent noise amplification (1). In CS-SENSE, the *g*-factor indicates the amplification of both noise and artifacts due to undersampling from the first step of SparseMRI. Because the *g*-factor usually increases with the SENSE reduction factors, the error propagation becomes serious when R_2 is large. Figure 9 shows the error propagation with $R_2 = 2$ and $R_2 = 4$ in the noise-free simulation. In this figure, although the errors are undetectable in both aliased images with $R_1 = 2$, they are amplified in the SENSE step more with $R_2 = 4$ than with $R_2 = 2$. Because the *g*-factor for $R_2 = 4$ is larger and more spatially nonuniform, the error becomes more visible and nonuniformly distributed in the reconstruction.

Due to the abovementioned error propagating property of CS-SENSE, proper choice of the R_1 and R_2 pair is crucial for high-quality reconstruction. Figure 10 compares the reconstruction quality with different combinations of R_1 and R_2 for the same net reduction factors: $R = 4$ (2×2, 1×4), $R = 6$ (3×2, 2×3), $R = 8$ (4×2, 2×4). This figure suggests that a large R_1 will result in more artifacts (e.g., $R_1 = 4$) and a large R_2 will result in large error/noise amplification ($R_2 = 4$). When the image is sparse, a large factor of R_1 is preferred; when the *g*-factor is small, a large factor of R_2 is preferred. This observation could be a guideline for selection of the reduction factors R_1 andR_2 in practice, given the noise level and SENSE *g*-factor. The reduction factors in SparseMRI and SENSE should be balanced to minimize the final reconstruction error.

Computational Complexity

The current implementation of CS-SENSE and SparseMRI followed by SoS needs longer execution time than SparseSENSE due to more computations channel by channel. For example, when reconstructing a brain image with a reduction factor 4, CS-SENSE, SparseSENSE, SparseMRI followed by SoS, and VD-SENSE with ℓ_2 regularization took 183.6 sec, 111.9 sec, 240.4 sec, and 55.9 sec, respectively. This drawback of CS-SENSE can be overcome by parallel computing using a multiprocessor or dedicated hardware systems. Because the *k*-space data are acquired from multiple channels simultaneously in pMRI and reconstruction of the aliased images at each channel is independent, the SparseMRI procedure in CS-SENSE can be performed simultaneously for all channels. Thus, the computational time of CS-SENSE can be reduced to be approximately the same as that of VD-SENSE with ℓ_2 regularization, and less than that of SparseSENSE. The computational time of additional Cartesian SENSE (3.9 sec) is negligible compared to the iterative algorithms used for SparseMRI and can be accelerated using commodity graphics hardware (29).

Extensions

In CS-SENSE, ℓ_1 minimization is used in the CS step. Recently, ℓ_p minimization ($0 < p < 1$) and approximated ℓ_0 minimization have been proposed for CS reconstruction and shown to require less computation time (30-32). These minimization methods may also be used in the CS step of the proposed method to speed up reconstruction.

Another possible extension of CS-SENSE is to utilize the correlations among aliased images. In CS-SENSE, the aliased images of all channels are reconstructed indepen-

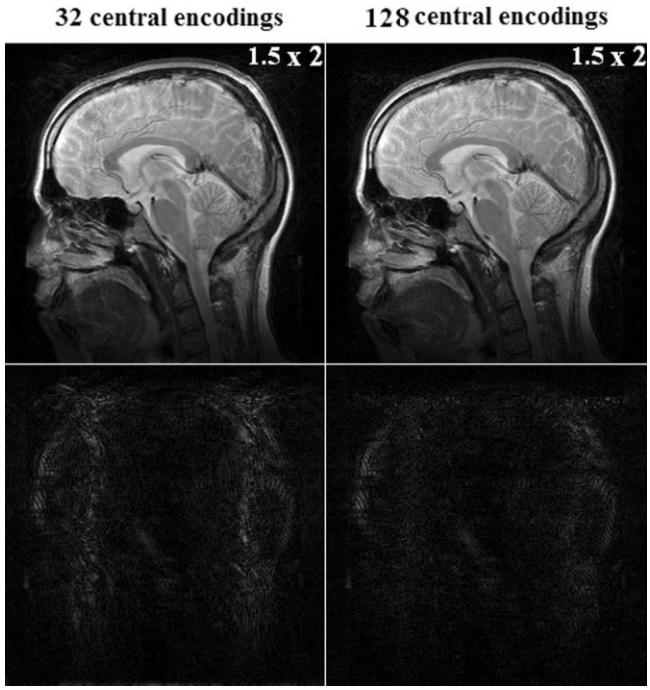

FIG. 8. CS-SENSE reconstructions of the sagittal image ($R = 1.5 \times 2$) in Fig. 6 using sensitivity profiles estimated from 32 and 128 central encodings.

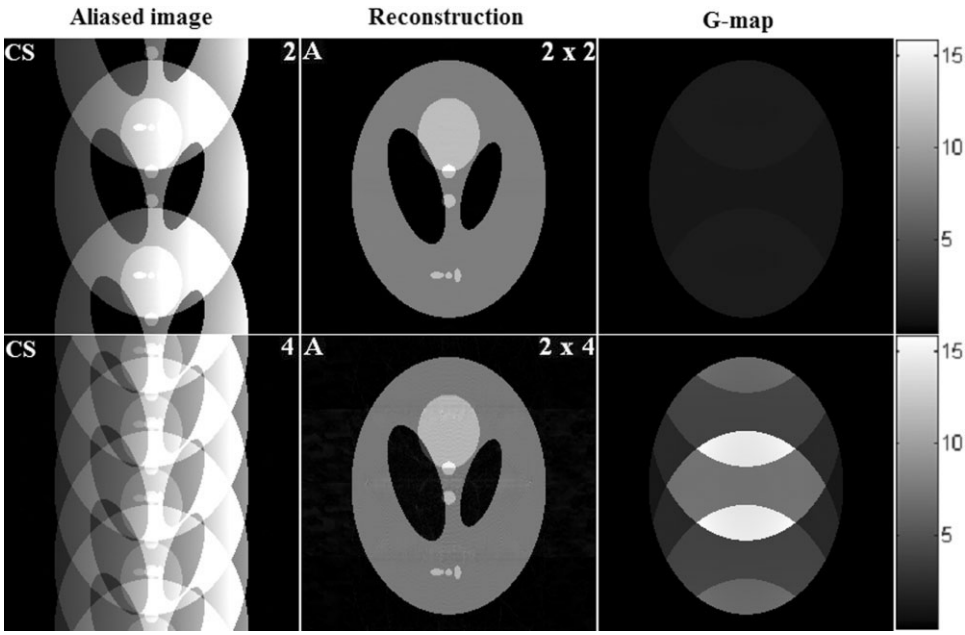

FIG. 9. The SparseMRI reconstructed aliased images (left column) have undetectable errors with $R_1 = 2$. The final CS-SENSE reconstructions (middle column) show more artifacts with $R_2 = 4$ than with $R_2 = 2$. This is because the different *g*-factor maps in the second SENSE step (right column) amplify the similar errors from the first SparseMRI step differently.

dently without taking advantage of their correlations. Actually, the aliased images from all channels share the common sparse support in the sparsifying transform domain. Distributed CS (DCS) is an extension of CS for simultaneous reconstruction of multiple signals with intra- and intersignal correlations (33). With distributed CS algorithms (34-36), all aliased images with common sparse support may be simultaneously reconstructed using fewer samples. Some preliminary work has been done (37,38).

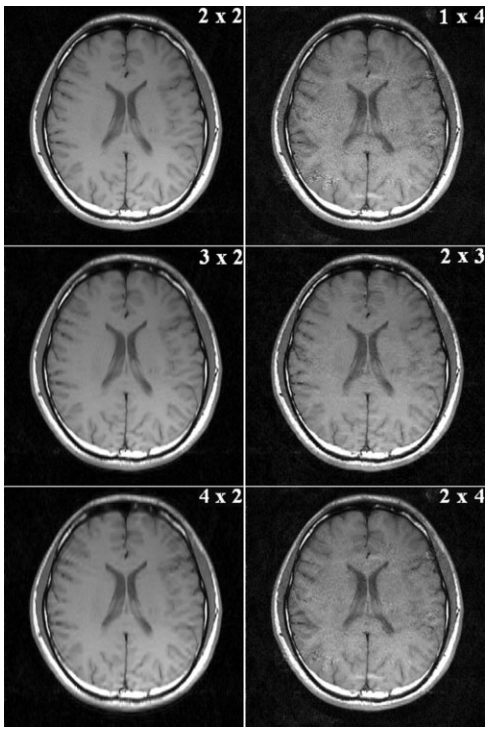

FIG. 10. CS-SENSE reconstructions of the axial image in Fig. 4, with different combinations of reduction factors.

The CS-SENSE results have shown that the reduction factor for the SENSE step should be kept as low as $R_2 = 2$ to avoid large noise amplification due to ill-conditioned SENSE. To increase R_2 for higher reduction, regularization techniques suitable for Cartesian SENSE (39–42) may also be incorporated into the SENSE step of CS-SENSE.

The current formulation of CS-SENSE can only be used for Cartesian trajectories. Future work will also explore the extension of CS-SENSE for non-Cartesian trajectories.

ACKNOWLEDGMENTS

This work was supported in part by the National Science Foundation CBET-0731226 and UWM Research Foundation. The authors thank Michael Lustig for making available the SparseMRI MATLAB code at http://www.stanford.edu/~mlustig/SparseMRI.html. The authors also thank the anonymous reviewers for their invaluable comments, which improved the quality of this study.

REFERENCES

1. Pruessmann KP, Weiger M, Scheidegger MB, Boesiger P. SENSE: sensitivity encoding for fast MRI. Magn Reson Med 1999;42:952–962.
2. Sodickson DK, Manning WJ. Simultaneous acquisition of spatial harmonics (SMASH): fast imaging with radiofrequency channel arrays. Magn Reson Med 1997;38:591–603.
3. Griswold MA, Jakob PM, Heidemann RM, Nittka M, Jellus V, Wang J, Kiefer B, Haase A. Generalized autocalibrating partially parallel acquisitions (GRAPPA). Magn Reson Med 2002;47:1202–1210.
4. Candès EJ, Romberg J, Tao T. Robust uncertainty principles: exact signal reconstruction from highly incomplete frequency information. IEEE Trans Inf Theory 2006;52:489–509.
5. Donoho D. Compressed sensing. IEEE Trans Inf Theory 2006;52:1289–1306.
6. Candès EJ, Romberg J. Sparsity and incoherence in compressed sampling. Inverse Problems 2007;23:969–985.
7. Candès EJ, Wakin M. An introduction to compressive sampling. IEEE Signal Processing Magazine 2008;25:21–30.
8. Candès EJ, Romberg J, Tao T. Stable signal recovery from incomplete and inaccurate measurements. Commun Pure Appl Math 2006;59:1207–1223.

9. Haupt J, Nowak R. Signal reconstruction from noisy random projections. IEEE Trans Inf Theory 2006;52:4036–4048.
10. Lustig M, Donoho DL, Pauly JM. Sparse MRI: the application of compressed sensing for rapid MR imaging. Magn Reson Med 2007;58:1182–1195.
11. Block KT, Uecker M, Frahm J. Undersampled radial MRI with multiple channels: iterative image reconstruction using a total variation constraint Magn Reson Med 2007;57:1086–1098.
12. Ye JC, Tak S, Han YJ, Park HW. Projection reconstruction MR imaging using FOCUSS. Magn Reson Med 2007;57:764–775.
13. Liu B, Sebert FM, Zou Y, Ying L. SparseSENSE: randomly-sampled parallel imaging using compressed sensing. In: Proceedings of the 16th Annual Meeting of ISMRM, Toronto, 2008. p 3154.
14. Zhao C, Lang T, Ji J. Compressed sensing parallel imaging. In: Proceedings of the 16th Annual Meeting of ISMRM, Toronto, 2008. p 1478.
15. Wu B, Millane RP, Watts R, Bones P. Applying compressed sensing in parallel MRI. In: Proceedings of the 16th Annual Meeting of ISMRM, Toronto, 2008. p 1480.
16. King KF. Combining compressed sensing and parallel imaging. In: Proceedings of the 16th Annual Meeting of ISMRM, Toronto, 2008. p 1488.
17. Liang D, Liu B, Ying L. Accelerating sensitivity encoding using compressed sensing. In: Proceedings of the 30th Annual International Conference of the IEEE Engineering in Medicine and Biology Society, Vancouver, 2008. p 1667–1670.
18. Pruessmann KP, Weiger M, Börnert P. Advances in sensitivity encoding with arbitrary *k*-space trajectories. Magn Reson Med 2001;46:638–651.
19. Lustig M, Donoho DL, Santos JM, Pauly JM. Compressed Sensing MRI. IEEE Signal Processing Magazine 2008;25:72–82.
20. Radin L, Osher S, Fatemi E. Non-linear total variation noise removal algorithm. Phys D 1992;60:259–268.
21. Hoge WS, Brooks DH, Madore B, Kyriakos WE. A tour of accelerated parallel MR imaging from a linear systems perspective. Concepts Magn Reson Part A 2005;27A:17–37.
22. Ying L, Sheng J. Joint image reconstruction and sensitivity estimation in SENSE (JSENSE). Magn Reson Med 2007;57:1196–1202.
23. Ulaby FT. Fundamentals of applied electromagnetics. 5th edition. Prentice Hall; 2006.
24. Bernstein MA, King KF, Zhou X-H. Handbook of MRI pulse sequence. Academic Press; 2004.
25. Madore B. Unfold-SENSE: a parallel MRI method with self-calibration and artifact suppression. Magn Reson Med 2004;52:310–320.
26. Ying L, Liu B, Steckner MK, Wu G, Wu M, Li S-J. A statistical approach to SENSE regularization with arbitrary trajectories. Magn Reson Med 2008;60:414–421.
27. Marinelli L, Hardy CJ, Blezek DJ. MRI with accelerated multi-channel compressed sensing. In: Proceedings of the 16th Annual Meeting of ISMRM, Toronto, 2008. p 1484.
28. Daubechies I. Ten lectures on wavelets. Philadelphia: Siam Press; 1992.
29. Hansen MS, Atkinson D, Sorensen TS. Cartesian SENSE and k-t SENSE reconstruction using commodity graphics hardware. Magn Reson Med 2008;59:463–468.
30. Chartrand R. Exact reconstruction of sparse signals via nonconvex minimization. IEEE Signal Processing Lett 2007;14:707–710.
31. Fischer A, Breuer F, Blaimer M, Seiberlich N, Jakob PM. Introduction of a nonconvex compressed sensing algorithm for MR imaging. In: Proceedings of the 16th Annual Meeting of ISMRM, Toronto, 2008. p 1487.
32. Trzasko JD, Manduca A. A highly undersampled magnetic resonance image reconstruction via homotopic ℓ_o-minimization. IEEE Trans Med Imaging 2009;28:106–121.
33. Duarte MF, Wakin MB, Baron D, Baraniuk RG. Universal distributed sensing via random projections. In: ACM/IEEE International Conference on Information Processing in Sensor Networks, 2006. p 177–185.
34. Cotter SF, Rao BD, Engan K, Kreutz-Delgado K. Sparse solutions to linear inverse problems with multiple measurement vectors. IEEE Trans Signal Processing 2005;53:2477–2488.
35. Tropp JA, Gilbert AC, Strauss MJ. Algorithms for simultaneous sparse approximation, part I: greedy pursuit. Signal Processing 2006;86:572–588.
36. Tropp JA, Gilbert AC, Strauss MJ. Algorithms for simultaneous sparse approximation, part II: convex relaxation. Signal Processing 2006;86:589–602.
37. Liang D, King KF, Liu B, Ying L. Accelerated parallel MRI using M-FOCUSS. In: ISMRM Workshop on Data Sampling and Image Reconstruction, 2009.
38. Liang D, King KF, Liu B, Ying L. Accelerated SENSE using distributed compressed sensing. In: Proceedings of the 17th Annual Meeting of ISMRM, Honolulu, 2009.
39. Lin F-H, Kwong KK, Belliveau JW, Wald LL. Parallel imaging reconstruction using automatic regularization. Magn Reson Med 2004;51:559–567.
40. Ying L, Xu D, Liang Z-P. On Tikhonov regularization for image reconstruction in parallel MRI. In: Proceedings of the 26th Annual International Conference of the IEEE EMBS, San Francisco, 2004. p 1056–1059.
41. King KF. SENSE image quality improvement using matrix regularization. In: Proceedings of the 9th Annual Meeting of the ISMRM, Glasgow, Scotland, 20091. p. 1771.
42. Liang Z-P, Bammer R, J. J, Pelc N, Glover G. Making better SENSE: wavelet de-noising, Tikhonov regularization, and total-least squares. In: Proceedings of the 10th Annual Meeting of the ISMRM, Honolulu, HI, 20902. p. 2388.